Journal of Power Sources 196 (2011) 8561–8567

Contents lists available at ScienceDirect

Journal of Power Sources

journal homepage: www.elsevier.com/locate/jpowsour

Effect of impregnation phases on the performance of Ni-based anodes for low temperature solid oxide fuel cells

Zhangbo Liu[a], Dong Ding[b], Beibei Liu[a], Weiwei Guo[a], Wendong Wang[c], Changrong Xia[a,*]

[a] CAS Key Laboratory of Materials for Energy Conversion, Department of Materials Science and Engineering, University of Science and Technology of China, Hefei, 230026 Anhui, China
[b] School of Materials Science and Engineering, Georgia Institute of Technology,771 Ferst Drive NW, Atlanta, GA 30332, United States
[c] Department of Chemical Physics, University of Science and Technology of China, Hefei, 230026 Anhui, China

ARTICLE INFO

Article history:
Received 27 April 2011
Received in revised form 26 May 2011
Accepted 26 May 2011
Available online 25 June 2011

Keywords:
Wet impregnation technique
Catalytic activity
Triple-phase-boundary
Ceria
Solid oxide fuel cells

ABSTRACT

Impregnated nanoparticles are very effective in improving the electrochemical performance of solid oxide fuel cell (SOFC) anodes possibly due to the extension of reaction sites and/or the enhancement of catalytic activity. In this work, samaria-doped ceria (SDC), pure ceria, samaria, and alumina oxides impregnated Ni-based anodes are fabricated to compare the site extending and the catalytic effects. Except for alumina, the impregnation of the other three nano-sized oxides could substantially enhance the performance of the anodes for the hydrogen oxidation reactions. Moreover, single cells with CeO_2 and Sm_2O_3 impregnated anodes could exhibit as great performance as those with SDC impregnated anodes. When the impregnation loading reached the optimal value, 1.7 mmol cm^{-3}, these cells exhibit very high performance, with peak power densities around 750 mW cm^{-2}. The high performance of CeO_2 and Sm_2O_3 impregnated anodes demonstrates that the improved performance are mainly attributed to the significantly improved electrochemical activities of the anodes, but not to the extension of triple-phase-boundary, and wet impregnation is indeed an alternative and effective technique to introduce these nano-sized catalytic active oxides into the anode configuration of SOFCs to enhance cell performance, stability and reliability.

1. Introduction

Solid oxide fuel cell (SOFC) is an all solid energy conversion device which can directly convert chemical into electrical energy with high efficiency and very low greenhouse emission. SOFC development has been booming worldwide for many decades, which should be attributed to continuous optimizations in materials, cell design, and manufacturing processing. Recently, there have been lots of interests in improving the performance of electrodes to reduce the operation temperature of SOFC systems [1].

It has been shown that ion impregnation is an effective way to introduce nano-sized oxide particles into anode configuration at relatively low temperatures [2,3]. Jiang et al. have shown that the performance of Ni-based anodes can be substantially improved by impregnating nano-sized yttria-stabilized zirconia (YSZ) or gadolinia-doped ceria (GDC) [2,4–6]. The nano-sized oxide particles are believed to extend the reaction zone, resulting in significant increase in the electrochemical activities of the Ni-based cermet anodes for the hydrogen oxidation reaction [2]. In addition, the nano-sized GDC particles have even exhibited very high activity towards the re-oxidation of deposited carbon on the Ni surface probably through the effective distribution and dispersion of oxygen ions, as compared to the GDC phase in the Ni-GDC cermet anodes [6]. Gorte's research group has successfully fabricated Ni-free Cu-based composite anodes utilizing the wet impregnation technique [7–17]. The anodes are composites of copper, ceria and YSZ, among which both the copper and ceria are introduced into the YSZ framework via the wet impregnation technique. In this anode formulation, ceria is used as an oxidation catalyst, while copper provides electronic conductivity [7,9]. These anodes have shown very exciting performance for utilization of hydrogen and many hydrocarbon fuels, suggesting that impregnated nano-sized particles are highly active in catalyzing the anodic reactions [7,10,12,14–16].

In our laboratory, there also have been lots of previous studies towards improvement of the Ni-based anodes by means of impregnating nano-sized samaria-doped ceria (SDC) into the anode substrates [18–23]. In these anodes, the direct contact between the Ni particles and hydrocarbon fuel is well blocked by the coated SDC nanoparticles, so that carbon deposition is effectively suppressed, and the cells could represent great performance and stability when methane as well as *iso*-octane is used as the fuel [18,21,22]. Moreover, compared with the cells without any impregnation treatment, distinct improvement in performance is observed for the cells with such SDC-coated anodes when hydrogen is used as the fuel,

* Corresponding author. Tel.: +86 5513607475; fax: +86 5513606689.
E-mail address: xiacr@ustc.edu.cn (C. Xia).

0378-7753/$ – see front matter © 2011 Elsevier B.V. All rights reserved.
doi:10.1016/j.jpowsour.2011.05.076

which may be attributed to an effective extension of the triple-phase-boundary (TPB), as demonstrated by the model comparison and relative experimental investigation [18–20]. In summary, impregnated nanoparticles seem very promising in achieving high performance for low temperature operation, as well as for the direct utilization of hydrocarbon fuels.

Previous investigation has shown that the improved electrochemical performance may be attributed either to the extension of TPB as demonstrated by Jiang et al. and our work, or to the enhanced catalytic activity of ceria as proved by Gorte et al. Since doped ceria has high oxygen ion conductivity and is also an excellent oxidation catalyst, it is possible that the improvement is caused by both extending TPB and enhancing catalytic activity. Nevertheless, there is urgent need to compare the two effects so as to direct the development of impregnated anodes.

The goal of the present study is to compare the two effects by characterizing Ni-based anodes impregnated with different oxide nanoparticles of SDC, ceria, samaria, and alumina. SDC is an excellent oxygen ion conductor and also catalytic active. Ceria is an outstanding catalyst and also an oxygen ion conductor in reducing atmosphere due to the transformation of Ce^{4+} to Ce^{3+}. Samaria is not a good conductor but has been lately reported to be highly active in a novel Ni–Sm_2O_3 cermet anode [24]. And alumina is neither a conductor nor a catalytic.

2. Experimental

2.1. Powder synthesis

All the powders involved in this work including $Sm_{0.2}Ce_{0.8}O_{1.9}$ (SDC), NiO and $Sm_{0.5}Sr_{0.5}CoO_3$ (SSC) were synthesized via glycine–nitrate process (GNP). Taking the synthesis of SDC powders as an example, certain stoichiometric amount of $Sm(NO_3)_3$ and $Ce(NH_4)_2(NO_3)_6$ to the nominal composition of SDC was dissolved into distilled water to form a mixed nitrate solution, in which glycine was added as complexing agent, with the molar ratio of glycine:NO_3^- = 1:2. After stirring for about 30 min, the solution was heated on a hotplate till rapid self-sustaining combustion, and the resulted ashes were calcined at 600 °C for 2 h to form fluorite phase SDC powders. In the case of NiO as well as SSC synthesis, the resulted ashes were both calcined at 850 °C for 4 h to get the desired oxides.

2.2. Cell fabrication and impregnation processing

Bi-layer pellets consisted of porous NiO–SDC substrates and dense SDC electrolytes were fabricated by combined co-pressing and co-sintering process [25]. NiO and SDC powders were mixed to form the precursor of the anode substrate, in which graphite was also added to increase the porosity, which is critical for the following ion-impregnation process. The mass ratio of NiO, SDC and graphite was 9:1:2. It should be noted that the addition of small amount of SDC was to enhance thermal and chemical compatibility between the substrate and the electrolyte, but not to provide a continuous ion conducting path. The mixed powders were compacted at 50 MPa. Then a thin layer of SDC powder was uniformly distributed onto the pre-pressed substrate and uniaxially co-pressed to 300 MPa to form green bi-layer pellets, which were subsequently co-sintered at 1250 °C for 5 h to densify the SDC electrolytes. The sintered substrate thickness and diameter were 0.480 mm and 11.2 mm, respectively, while the thickness of the dense electrolyte was about 32.3 μm. The porosity of the anode substrate was 36%, which was measured by the Archimedes method.

All of the impregnation solutions including $Sm_{0.2}Ce_{0.8}(NO_3)_3$, $Ce(NO_3)_3$, $Sm(NO_3)_3$ and $Al(NO_3)_3$ were prepared by dissolving the corresponding nitrates into distilled water, with the same total cation concentration of 1.0 mol L^{-1}. For convenience, the cells with anodes impregnated by each solution are designated as FC-SDC, FC-CeO_2, FC-Sm_2O_3, and FC-Al_2O_3 thereinafter. Each solution was dropped onto the porous anode substrates of the sintered half cells under vacuum, and the droplets were allowed to infiltrate the anode framework by capillary action. After drying, the pellets were fired at 800 °C for 2 h to decompose the nitrate salts and form corresponding metal oxides. The loading of the impregnated oxides were estimated by measuring the weight differences before and after each impregnation-heating treatment. The impregnation-heating cycle was repeated to increase the loading to an expected value. The loadings for FC-SDC, FC-CeO_2, FC-Sm_2O_3, and FC-Al_2O_3 at different cycles are listed in Table 1, in which the loadings are expressed as 10^{-3} mol oxide per volume substrate, mmol cm^{-3}. It can be seen clearly that at the same impregnation cycle, the loading is almost the same to each other, which may be attributed to the same total cation concentration, 1.0 mol L^{-1}, as well as the same anode framework. And for a given oxide such as SDC, the loading decreases slightly with cycle number due to the decreased porosity of the substrate after each cycle.

Table 1
Loading (mmol cm^{-3}) for FC-SDC, FC-CeO_2, FC-Sm_2O_3 and FC-Al_2O_3 after different impregnation-heating cycles.

Sample	Cycle	Loading	Sample	Cycle	Loading
FC-SDC-2	2	0.956	FC-CeO_2-2	2	0.958
FC-SDC-3	3	1.41	FC-CeO_2-3	3	1.41
FC-SDC-4	4	1.71	FC-CeO_2-4	4	1.72
FC-SDC-5	5	2.10	FC-CeO_2-5	5	2.11
FC-Sm_2O_3-2	2	0.946	FC-Al_2O_3-1	1	0.496
FC-Sm_2O_3-3	3	1.39	FC-Al_2O_3-2	2	0.954
FC-Sm_2O_3-4	4	1.70	FC-Al_2O_3-3	3	1.41
FC-Sm_2O_3-5	5	2.09	FC-Al_2O_3-4	4	1.82

After completing the impregnation process, cathodes were applied. SSC–SDC composite powders with the weight ratio of SSC:SDC = 7:3 were mixed thoroughly with 10 wt% ethylcellulose–terpineol binder to form the cathode slurry, which was subsequently screen-printed onto the electrolyte surface, followed by co-firing at 950 °C for 2 h to complete the whole single cells. The cathode was printed at the center of the pellet and had a diameter of 8.0 mm. The whole process was kept as consistent as possible so that identical cathodic polarization resistance could be achieved [18,26].

2.3. Cell testing and characterization

Each single cell was sealed onto an alumina tube with silver paste (DAD-87, Shanghai Research Institute of Synthetic Resins), placed inside a vertical furnace, and heated to 600 °C for electrochemical characterization. Humidified (3% H_2O) hydrogen was fed to the anode at a flow rate of 50 mL min^{-1} as the fuel, while ambient air was employed as the oxidant at the cathode side. An Electrochemical Workstation (IM6e, Zahner) was used to investigate the cell performance. In addition to measuring the current–voltage curve using the galvanostatic mode, the electrochemical impedance spectra were measured under open circuit condition in the frequency range from 0.1 Hz to 1 MHz with an AC amplitude of 10 mV. The microstructure was observed via a scanning electron microscopy (SEM, JSM-6700F, JEOL).

In order to characterize the catalytic activity of these anodes with various kinds of impregnation phase, temperature programmed reduction (TPR) measurements were carried out in a conventional system equipped with a thermal conductivity detector, as described in detail elsewhere [27]. The samples for TPR measurements were grinded into small particles with an average

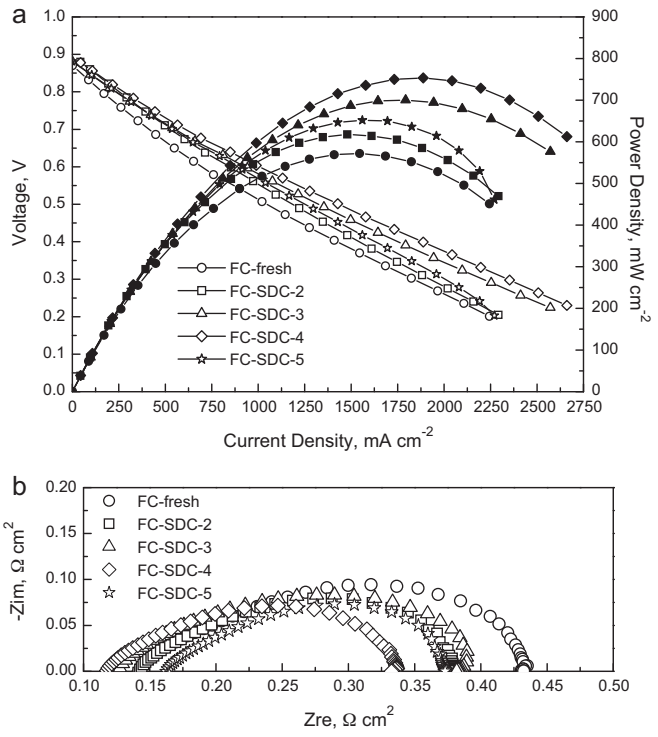

Fig. 1. (a) Dependence of cell voltage and power density on current density and (b) impedance spectra measured under open circuit conditions, for FCs-SDC with different amount of SDC loadings tested at 600 °C, when humidified H_2 (3% H_2O) and ambient air were used as the fuel and the oxidant, respectively.

diameter of 0.25–0.5 mm, and for each measurement ~50 mg of the samples were used. After pretreated in a flow of pure Ar at 400 °C for 30 min, the reduction was performed in a flow of 5% H_2/Ar (with a flowing rate of 30 mL min^{-1}) from 100 °C to 900 °C with a heating rate of 5 °C min^{-1}. The amount of hydrogen consumption during the measurement was estimated from the integrated peak areas with CuO as a standard.

3. Results and discussions

3.1. Fuel cells performance

3.1.1. Single cells with SDC impregnated anodes

Fig. 1a shows typical current–voltage curves for FCs-SDC with different SDC loading. The measurement was conducted at 600 °C, using humidified H_2 (3% H_2O) and ambient air as the fuel and the oxidant, respectively. The performance of the fresh cell (designated as FC-fresh thereinafter), whose anode is not impregnated with any oxides, is also shown for comparison. Each cell exhibits an open circuit voltage (OCV) between 0.87 V and 0.89 V, which are typical for SOFCs with SDC electrolytes and SSC–SDC cathodes at the same temperature [28]. The cell performance changes obviously with SDC loading. FC-fresh represents a peak power density of 572 mW cm^{-2}, much higher than the value of the cell prepared using 20 wt% starch as pore former [18,20], indicating that graphite appears to be a more effective pore former than starch in optimizing the anode microstructure. Furthermore, cell performance increases markedly with the loading, i.e., peak power densities as high as 618 and 700 mW cm^{-2} are achieved with the loading of 0.956 and 1.41 mmol cm^{-3}, respectively. When the SDC loading further increases to 1.71 mmol cm^{-3} after four cycles of impregnation-heating treatment, peak power density increases to 754 mW cm^{-2}, which is the highest of these SDC impregnated cells. Further increasing the loading, however, leads to a decrease of the cell performance, i.e., only 652 mW cm^{-2} of the peak power density is obtained with 2.10 mmol cm^{-3} loading at five cycles, even lower than that of FC-SDC-3. Such tendency of the cell performance versus impregnated SDC loading is basically consistent with the previous work using starch as the pore former [20].

Fig. 1b shows the typical electrochemical impedance spectra for FCs-SDC measured under open circuit conditions at 600 °C using a two-electrode configuration. The ohmic resistance, R_{ohm}, corresponding to the high frequency intercept with the real axis, is primarily derived from the ion conducting resistance of the electrolyte and the interface contact resistance between the electrolyte and the electrodes, in spite of the negligible electron conducting resistance of both Ni based anode and SSC based cathode under the testing conditions. And the interfacial polarization resistance, R_p, determined from the difference between the high and low frequency intercepts with the real axis, is a combination of both the anodic and cathodic polarization resistances. It is difficult, however, to separate the anodic polarization resistance, R_a, from the cathodic one clearly, due to the complexity of the impedance spectra obtained with an anode-supported cell with a thin electrolyte [29]. Since the fabrication process of the SSC–SDC cathode is kept as consistent as possible, an equal cathodic polarization resistance can be assumed, indicating that the variation of R_p can be considered to be only derived from R_a.

As shown in Fig. 1b, R_p decreases from 0.288 Ω cm^2 for FC-fresh to 0.216 Ω cm^2 when 1.71 mmol cm^{-3} SDC is impregnated, with a reduction ratio of 25%. Moreover, the ohmic resistance is also reduced by the impregnation process within the critical loading corresponding to the highest peak power density. In the case of FC-fresh, R_{ohm} is 0.143 Ω cm^2, which decreases to 0.118 Ω cm^2 after 4 cycles of SDC impregnation. The reduction of R_{ohm} is possibly due to the extension of the contact area at the anode–electrolyte interface by the impregnated nano-sized SDC particles, as demonstrated by van Berkel et al. that smaller particles at the anode–electrolyte interface could bring in larger areas, which would cause faster reaction kinetics and higher currents that could be drawn through the electrode [30]. It is clear that the improvement of cell performance is related to the decrease of both R_a and R_{ohm} as an effect of nano-sized SDC impregnation treatment. In addition, it should be noted that when 2.10 mmol cm^{-3} SDC is loaded, R_p is 0.208 Ω cm^2, lower than the value of FC-SDC-4, but R_{ohm} increases to 0.163 Ω cm^2, leading to a much lower peak power density of only 652 mW cm^{-2}.

3.1.2. Single cells with ceria impregnated anodes

Fig. 2a shows the typical current–voltage curves for FCs-CeO_2 with different ceria loading. A similar tendency of the cell performance versus impregnation loading is observed for FCs-CeO_2 to that of FCs-SDC. As shown in Fig. 2a, 646 and 704 mW cm^{-2} of peak power densities are obtained with cells that suffer two and three cycles of ceria impregnation, respectively. When 1.72 mmol cm^{-3} ceria is coated, FC-CeO_2-4 demonstrates the best performance with 767 mW cm^{-2} of the peak power density. Further increase the loading such as 2.11 mmol cm^{-3} for FC-CeO_2-5 would degrade the cell performance.

Typical electrochemical impedance spectra for FCs-CeO_2 also behave the same tendency to that of FCs-SDC versus impregnation loading, as shown in Fig. 2b. Both the ohmic resistance and the interfacial polarization resistance are reduced by the nano-sized ceria loading within the optimal value that represents the best performance. For FC-CeO_2-4, which produces the highest peak power density, R_p is as low as 0.160 Ω cm^2, even lower than that of FC-SDC-4, while R_{ohm} is 0.110 Ω cm^2, very close to the value of FC-SDC-4. It can also be drawn from Fig. 2b that, too much ceria loading such as 2.11 mmol cm^{-3} by five cycles of impregnation treatment,

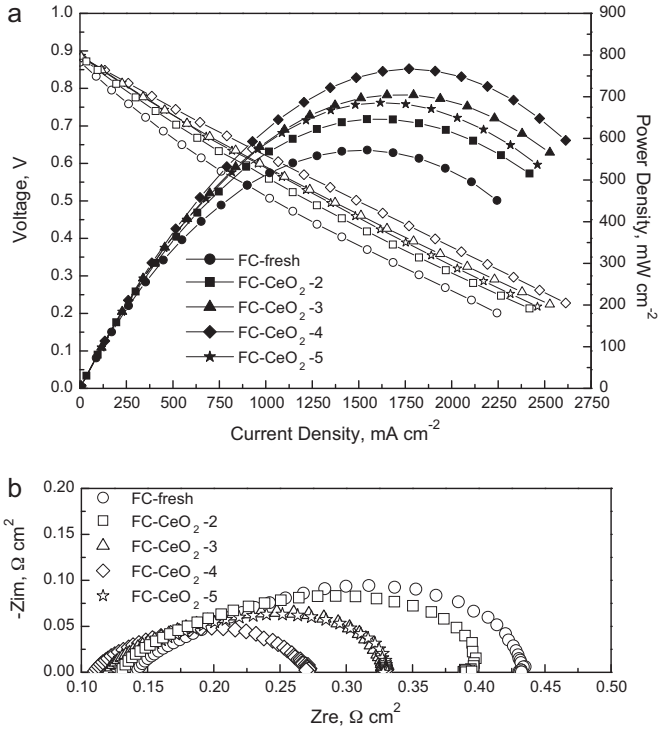

Fig. 2. (a) Dependence of cell voltage and power density on current density and (b) impedance spectra measured under open circuit conditions, for FCs-CeO_2 with different amount of CeO_2 loadings tested at 600 °C, when humidified H_2 (3% H_2O) and ambient air were used as the fuel and the oxidant, respectively.

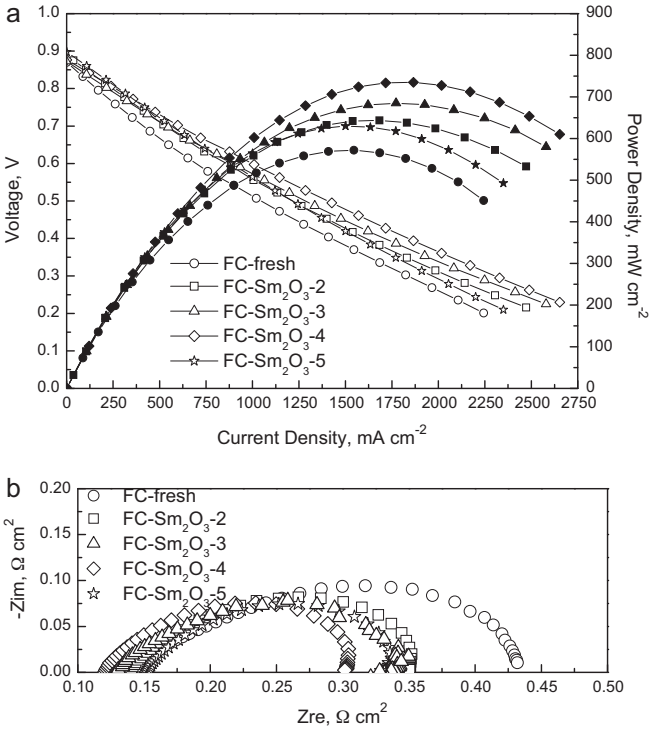

Fig. 3. (a) Dependence of cell voltage and power density on current density and (b) impedance spectra measured under open circuit conditions, for FCs-Sm_2O_3 with different amount of Sm_2O_3 loadings tested at 600 °C, when humidified H_2 (3% H_2O) and ambient air were used as the fuel and the oxidant, respectively.

would cause the increase of both R_{ohm} and R_p, thus reducing the cell performance.

3.1.3. Single cells with samaria impregnated anodes

Samarium oxide, with a conductivity of three orders of magnitude lower than that of SDC at 500–800 °C, is also employed as an impregnation phase into the porous anode configuration for comparison. Fig. 3a shows typical current–voltage curves for single cells with different amount of samaria impregnated anodes tested at 600 °C. The tendency of the cell performance versus impregnation loading seems very close to that of the cells with SDC impregnated anodes as well. As high as 644 and 685 mW cm^{-2} of the peak power density are achieved when 0.946 and 1.39 mmol cm^{-3} samaria are impregnated into the anode framework, respectively. And after four cycles of impregnation treatment, the highest performance with 735 mW cm^{-2} of the peak power density is obtained. Further more impregnation treatment would result in the decrease of the cell performance, as demonstrated by the relatively poor performance of FC-Sm_2O_3-5.

Fig. 3b shows the typical electrochemical impedance spectra for FCs-Sm_2O_3 measured under open circuit conditions. It can be seen clearly that, both the ohmic resistance and the interfacial polarization resistance are reduced by the nano-sized samaria loading within the optimal value that represents the best performance, very similar to the tendency observed when ceria is employed as the impregnation phase. In the case of FC-Sm_2O_3-4, which exhibits the highest peak power density, R_{ohm} and R_p are 0.120 and 0.181 Ω cm^2, respectively. Compared with the values of FC-SDC-4, the ohmic resistance of FC-Sm_2O_3-4 is a little higher, while its interfacial polarization resistance is much lower. Additionally, as expected, excessive samaria loading increases the ohmic resistance, i.e., as high as 0.152 Ω cm^2 of R_{ohm} is achieved when 2.09 mmol cm^{-3} samaria is loaded.

3.1.4. Single cells with alumina impregnated anodes

The tendency of performance versus loading for the cells with different impregnation phase, including SDC, CeO_2 and Sm_2O_3, seems very close to each other. Moreover, all the three type cells with the optimal loading behave very similar peak power densities, which are around 750 mW cm^{-2}. Accordingly, it may be doubtable that whatever nano-sized oxide particles introduced into the traditional Ni-based anodes via the wet impregnation technique could improve the cell performance more or less. To get an accurate conclusion, the inert oxide alumina is also employed as an impregnation phase for comparison test.

Fig. 4a shows typical current–voltage curves for FCs-Al_2O_3 with different alumina loadings. It can be seen clearly that the cell performance experiences a sharp decrease with only once alumina impregnation; the peak power density of FC-Al_2O_3-1 is as low as 372 mW cm^{-2}. And the performance further decreases with the loading, i.e., only 304 mW cm^{-2} of the peak power density is obtained when 1.82 mmol cm^{-3} alumina is loaded after four cycles of impregnation treatment.

Fig. 4b shows the typical electrochemical impedance spectra measured under open circuit conditions at 600 °C. Only once alumina impregnation causes sharp increase of both R_{ohm} and R_p, indicating that the impregnated alumina particles not only block the electron conduction path but also reduce the reactive sites. In addition, increasing of the impregnation cycles exacerbates the negative impacts, thus resulting in the further increase of both R_{ohm} and R_p, as can be seen clearly from Fig. 4b. Hansen et al. also have proved that impregnated alumina nano-particles have a detrimental effect on the activity of the strontium substituted lanthanum manganite (LSM) based cathodes [31].

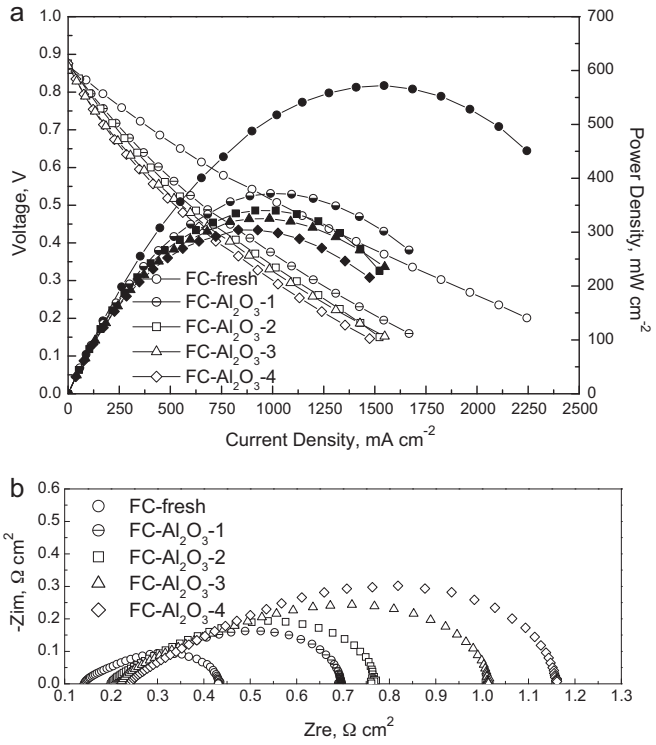

Fig. 4. (a) Dependence of cell voltage and power density on current density and (b) impedance spectra measured under open circuit conditions, for FCs-Al_2O_3 with different amount of Al_2O_3 loadings tested at 600 °C, when humidified H_2 (3% H_2O) and ambient air were used as the fuel and the oxidant, respectively.

3.2. Micro-structure of the impregnated anodes

Since the anode performance is very dependent on its microstructure [32], Fig. 5 compares the SEM pictures of the cross-sectional views of the anodes suffered four cycles of impregnation treatment. Fig. 5a shows that when the loading is 1.71 mmol cm^{-3}, except a few smooth Ni grains, the majority of Ni grains are covered by very fine and well dispersed nano-sized SDC particles, which have an average diameter of 40–60 nm. The microstructure of ceria impregnated anode appears to be very similar to that of SDC, as shown in Fig. 5b, and the particle size is estimated to be in the range of 40–60 nm as well. These well dispersed nano-sized SDC and CeO_2 particles are considered to be very important for the TPB extension within the anodes, as well as for the significant electro-catalytic activity towards hydrogen oxidation reaction. Fig. 5c displays the SEM image of anode impregnated with Sm_2O_3. The microstructure of this anode appears to be very different from those impregnated with SDC. In addition to granular particles which seem to be larger than those of SDC and CeO_2, rod-like protrusions (~200 nm in length and ~100 nm in diameter) are obviously observed, especially in the angular region of Ni grains. These peculiar protrusions, which are basically constituted with the loaded samaria particles, may become very high active areas towards electrode reactions, since samaria has been proved to be a good catalyst towards oxidation reactions [24]. Fig. 5d shows the cross-section morphology of the anode with alumina impregnation treatment. The size of alumina particles is close to that of the SDC and CeO_2 particles, but these particles are neither oxygen ion conductive nor electro-catalytic active towards oxidation reaction. Furthermore, as no significant change of the microstructure occurs after fuel cells testing, good stability and reliability of these impregnated anodes could be expected.

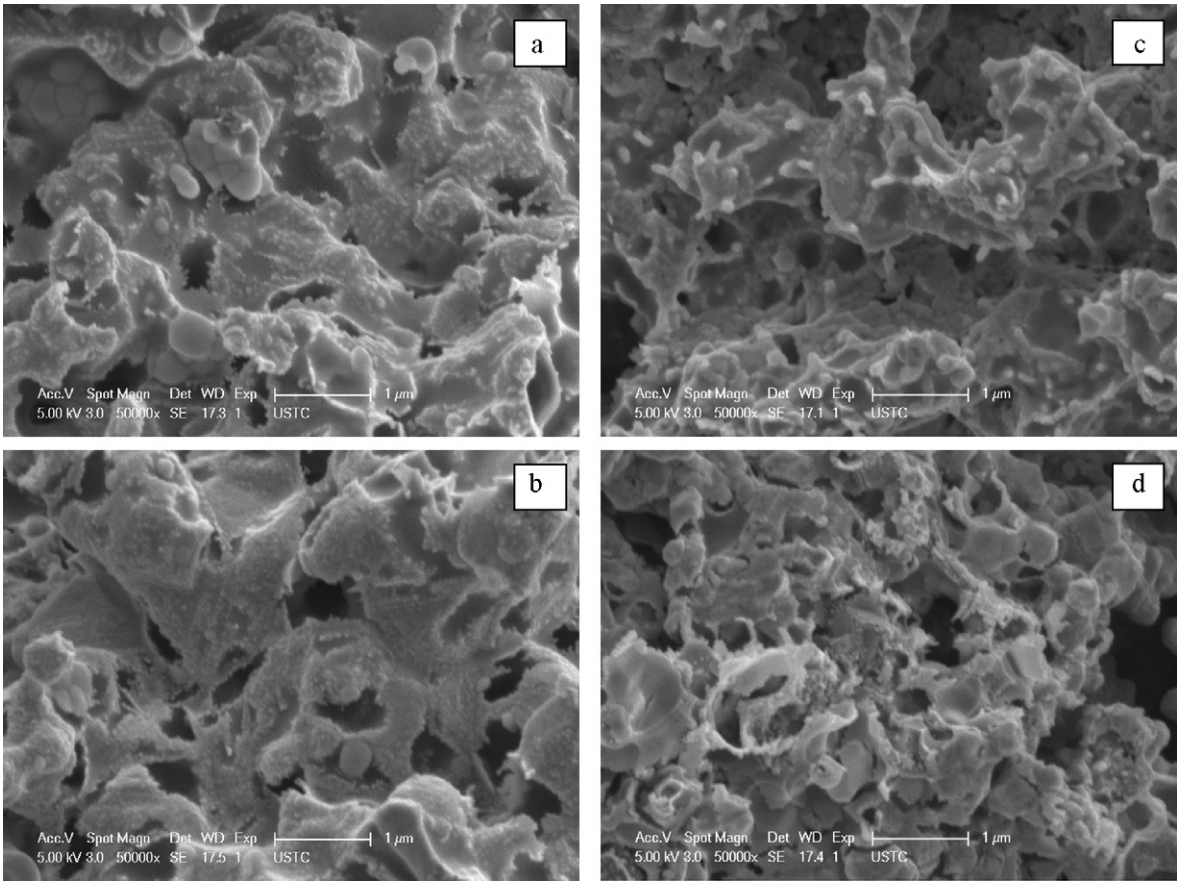

Fig. 5. SEM pictures of fractured cross-sections of impregnated anodes of: (a) FC-SDC-4, (b) FC-CeO_2-4, (c) FC-Sm_2O_3-4 and (d) FC-Al_2O_3-4.

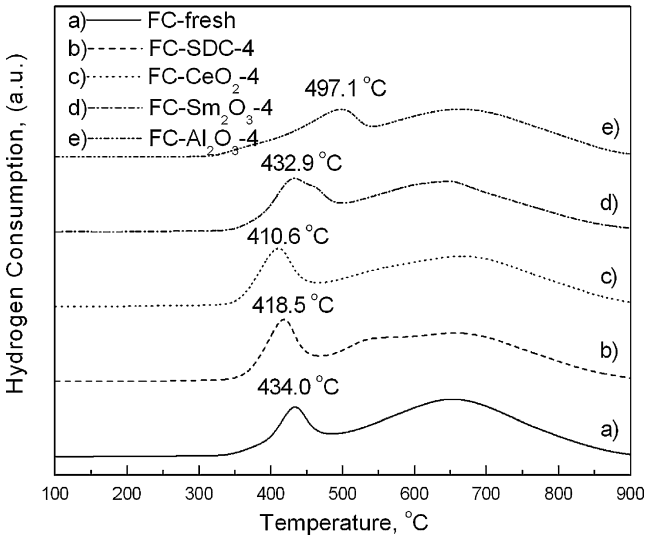

Fig. 6. H_2-TPR profiles for the anodes of cells: (a) FC-fresh, (b) FC-SDC-4, (c) FC-CeO_2-4, (d) FC-Sm_2O_3-4 and (e) FC-Al_2O_3-4, when 5% H_2/Ar was employed as the flowing gas.

3.3. H_2-TPR behavior of the impregnated anodes

Shown in Fig. 6 are the TPR profiles of the anodes of cells: (a) FC-fresh, (b) FC-SDC-4, (c) FC-CeO_2-4, (d) FC-Sm_2O_3-4 and (e) FC-Al_2O_3-4, when 5% H_2/Ar is employed as the flowing gas. As shown clearly in Fig. 6, the TPR profile of FC-fresh represents two separated peaks within the temperature range of 350–900 °C. Taking into account the fact that all the single cells were tested at 600 °C, the main issue of the TPR profile should be focused on the first peak appearing at around 434.0 °C, whereas the second one appears at around 650.0 °C, much higher than the cells operating temperature. When ~1.71 mmol cm^{-3} SDC or CeO_2 is loaded via the wet impregnation technique, the first peak shifts downward to 418.5 and 410.6 °C, respectively, indicating that nano-sized SDC and CeO_2 impregnation result in significantly improved catalytic activity of the anodes towards hydrogen oxidation reaction. In the case of the Sm_2O_3 impregnated anode, the profile appears to be very similar to that of the FC-fresh, thus indicating that the intrinsic catalytic activity of Sm_2O_3 towards hydrogen oxidation reaction is negligible. It can also be seen in Fig. 6 that alumina impregnation makes the first peak shift upward to as high as 497.1 °C, thus resulting in the decrease of the catalytic activity of the anode.

3.4. Discussions

As proposed by Jiang, the improved performances of ceria or doped ceria impregnated anodes are believed to be attributed to the extension of TPB by the loading of nanoparticles with sufficiently high ionic conductivity, in addition to their significant electro-catalytic effect on the electrochemical activity of the anode [33]. However, it is still not sure which effect is dominant.

It is well known that TPB, where electron conducting phase (i.e., Ni), ion conducting phase (i.e., SDC) and gas phase (i.e., hydrogen and product water vapor) meet, is the active site for electrochemical reaction in the composite electrode. When SDC or CeO_2 nanoparticles are impregnated into the anode framework, the TPB length is extended. As the ionic conductivity of pure ceria is much lower than that of SDC, the TPB extension for ceria impregnated anode is more limited. Since the performance of FCs-SDC and FCs-CeO_2 is similar, TPB extension is very likely not to be the dominant effect in enhancing the electrode activity.

On the other hand, both ceria and doped ceria are oxidation catalysts widely used in heterogeneous catalytic reactions [34]. Part of the cerium ions would transform from tetravalent (Ce^{IV}) to trivalent (Ce^{III}) under the high-temperature reducing conditions. The catalytic activity is considered to rely primarily on the activity of the redox couple Ce^{IV}–Ce^{III} with its ability to change from Ce^{IV} (CeO_2) under oxidizing conditions to Ce^{III} (Ce_2O_3) under net reducing conditions and vice versa. Ceria could be an essential catalyst towards various fuel oxidation reactions in SOFC anodes, as its redox properties could provide excellent oxygen-storage capacity [35]. The higher performance, especially the lower R_p value of FCs-CeO_2 in this work, may suggest that the significant electro-catalytic effect of the impregnated nanoparticles plays a dominant role on the improvement of anodes performance.

Furthermore, as can be seen clearly in Fig. 3, the single cells with samaria impregnated anodes exhibit as great performance as those with SDC or ceria modified anodes. It has also been demonstrated in our previous work that single cells with Ni–Sm_2O_3 composite anodes could generate very high performances, which are comparable to those with the conventional Ni–SDC composite anodes under the same operating conditions, when the same cathode and electrolyte are applied [24]. Since the conductivity of samarium oxide is three orders of magnitude lower than that of SDC at 500–800 °C, the high performance of FC-Sm_2O_3-4 must be attributed to improved activity towards anode reactions, as demonstrated by the lower R_p of FC-Sm_2O_3-4. The intrinsic activity of samaria towards hydrogen oxidation reactions, however, is proved to be much lower than that of ceria [34], indicating that the improved activity of the samaria impregnated anodes should not only be ascribed to the catalytic activity. Noting the fact that nickel itself originally has high catalytic properties towards fuel oxidation in the anode configuration, the improved activity may derive from the enhanced catalytic activity of nickel by the nano-sized samaria particles, possibly through a spillover effect, as proposed by Babaei et al. for the palladium particles modified Ni–GDC anodes [36], and also as demonstrated with Ni-Dy_2O_3 anodes [37].

The loading of alumina particles, which are neither oxygen ion conductive nor electro-catalytic active towards oxidation reaction, only has bad effect of blocking the electro conduction path and the reactive sites, thus resulting in the decrease of anode performance.

Thus, it can be concluded that the performance of the anode mainly depends on its catalytic activity, and wet impregnation technique is certainly an effective way to introduce nano-sized oxide particles with significantly high electro-catalytic activity into the anode framework. However, it should be noted that excessive loading may actually block the gas diffusion and electron conduction path in the anode, thus reducing the anode performance. Therefore, loading optimization is necessary for anodes consisting of different materials and with different porosity.

4. Conclusions

In this work, it has been demonstrated that single cells with CeO_2 or Sm_2O_3 impregnated anodes could exhibit as great performance as those with SDC impregnated anodes, with very high peak power densities which are around 750 mW cm^{-2}. Since the ionic conductivities of CeO_2 and Sm_2O_3 are much lower than that of SDC, the improved performances are believed to be mainly attributed to the significantly enhanced catalytic activities of the anodes, but not to the extension of TPB. In particular, for the Sm_2O_3 impregnated anodes, the improved activity may derive from the enhanced catalytic activity of nickel by the nano-sized Sm_2O_3 particles, possibly through a spillover effect. Although the catalytic activity of Sm_2O_3 impregnated anodes deserves further investigation in details, this work has proved that introducing nano-sized particles with sig-

nificantly high electro-catalytic activity through wet impregnation technique is one of the most effective approaches to design and develop anodes of SOFC for low temperature operation, as well as for the direct utilization of hydrocarbon fuels.

Acknowledgement

We gratefully acknowledge the financial support of the Natural Science Foundation of China (10979046 and 50730002).

References

[1] A. Atkinson, S. Barnett, R.J. Gorte, J.T.S. Irvine, A.J. Mcevoy, M. Mogensen, S.C. Singhal, J. Vohs, Nat. Mater. 3 (2004) 17.
[2] S.P. Jiang, Y.Y. Duan, J.G. Love, J. Electrochem. Soc. 149 (2002) A1175.
[3] S.P. Jiang, Y.J. Leng, S.H. Chan, K.A. Khor, Electrochem. Solid-State Lett. 6 (2003) A67.
[4] S.P. Jiang, S. Zhang, Y.D. Zhen, A.P. Koh, Electrochem. Solid-State Lett. 7 (2004) A282.
[5] S.P. Jiang, S. Zhang, Y.D. Zhen, W. Wang, J. Am. Ceram. Soc. 88 (2005) 1779.
[6] W. Wang, S.P. Jiang, A.I.Y. Tok, L.H. Luo, J. Power Sources 159 (2006) 68.
[7] R.J. Gorte, S. Park, J.M. Vohs, C.H. Wang, Adv. Mater. 12 (2000) 1465.
[8] R. Craciun, S. Park, R.J. Gorte, J.M. Vohs, C. Wang, W.L. Worrell, J. Electrochem. Soc. 146 (1999) 4019.
[9] S. Park, R.J. Gorte, J.M. Vohs, J. Electrochem. Soc. 148 (2001) A443.
[10] H. Kim, C. da Rosa, M. Boaro, J.M. Vohs, R.J. Gorte, J. Am. Ceram. Soc. 85 (2002) 1473.
[11] S. McIntosh, J.M. Vohs, R.J. Gorte, J. Electrochem. Soc. 150 (2003) A470.
[12] C. Lu, W.L. Worrell, C. Wang, S. Park, H. Kim, J.M. Vohs, R.J. Gorte, Solid State Ionics 152 (2002) 393.
[13] H.P. He, J.M. Vohs, R.J. Gorte, J. Electrochem. Soc. 150 (2003) A1470.
[14] R.J. Gorte, H. Kim, J.M. Vohs, J. Power Sources 106 (2002) 10.
[15] R.J. Gorte, J.M. Vohs, J. Catal. 216 (2003) 477.
[16] O. Costa-Nunes, R.J. Gorte, J.M. Vohs, J. Power Sources 141 (2005) 241.
[17] S.W. Jung, C. Lu, H.P. He, K. Ahn, R.J. Gorte, J.M. Vohs, J. Power Sources 154 (2006) 42.
[18] W. Zhu, C.R. Xia, J. Fan, R.R. Peng, G.Y. Meng, J. Power Sources 160 (2006) 897.
[19] W. Zhu, D. Ding, C.R. Xia, Electrochem. Solid-State Lett. 11 (2008) B83.
[20] D. Ding, W. Zhu, J.F. Gao, C.R. Xia, J. Power Sources 179 (2008) 177.
[21] D. Ding, Z.B. Liu, L. Li, C.R. Xia, Electrochem. Commun. 10 (2008) 1295.
[22] L.S. Zhang, J.F. Gao, R.F. Tian, C.R. Xia, Chin. J. Chem. Phys. 22 (2009) 429.
[23] L.S. Zhang, J.F. Gao, M.F. Liu, C.R. Xia, J. Alloys Compd. 482 (2009) 168.
[24] D. Ding, L. Li, K. Feng, Z.B. Liu, C.R. Xia, J. Power Sources 187 (2009) 400.
[25] C.R. Xia, M.L. Liu, Solid State Ionics 144 (2001) 249.
[26] Z. Xie, C.R. Xia, M.Y. Zhang, W. Zhu, H.T. Wang, J. Power Sources 161 (2006) 1056.
[27] W.D. Wang, P.Y. Lin, Y.L. Fu, C.Y. Cao, Catal. Lett. 82 (2002) 19.
[28] X.G. Zhang, M. Robertson, S. Yick, C. Deces-Petit, E. Styles, W. Qu, Y.S. Xie, R. Hui, J. Roller, O. Kesler, R. Maric, D. Ghosh, J. Power Sources 160 (2006) 1211.
[29] S. McIntosh, J.M. Vohs, R.J. Gorte, J. Electrochem. Soc. 150 (2003) A1305.
[30] F.P.F. van Berkel, F.H. van Heuveln, J.P.P. Huijsmans, Solid State Ionics 72 (1994) 240.
[31] K.K. Hansen, M. Wandel, Y.L. Liu, M. Mogensen, Electrochim. Acta 55 (2010) 4606.
[32] M. Mogensen, S. Skaarup, Solid State Ionics 86–88 (1996) 1151.
[33] S.P. Jiang, Mater. Sci. Eng. A Struct. Mater.: Prop. Microstruct. Process. 418 (2006) 199.
[34] A. Trovarelli, Catal. Rev. Sci. Eng. 38 (1996) 439.
[35] S. McIntosh, J.M. Vohs, R.J. Gorte, Electrochim. Acta 47 (2002) 3815.
[36] A. Babaei, S.P. Jiang, J. Li, J. Electrochem. Soc. 156 (2009) B1022.
[37] B.B. He, L. Zhao, W.D. Wang, F.L. Chen, C.R. Xia, Electrochem. Commun. 13 (2011) 194.